FULL PAPER

Enhanced effect of a plasma-irradiated titanium substrate on the photocatalytic activity of a TiO₂ film

Wei-Kun Zhu[1] (iD) | Kishor K. Kalathiparambil[1] | Zhi-Guang Sun[2] |
Chen-Yang Liu[2] | Ai-Min Zhu[2] (iD) | David N. Ruzic[1]

[1] Center for Plasma-Material Interactions, University of Illinois at Urbana Champaign, Urbana, Illinois 61801

[2] Laboratory of Plasma Physical Chemistry, Center for Hydrogen Energy and Environmental Catalysis, Dalian University of Technology, Dalian 116024, China

Correspondence
Wei-Kun Zhu, Center for Plasma-Material Interactions, University of Illinois at Urbana Champaign, Urbana, IL 61801.
Email: wzhu29@illinois.edu
Ai-Min Zhu, Laboratory of Plasma Physical Chemistry, Center for Hydrogen Energy and Environmental Catalysis, Dalian University of Technology, Dalian 116024, China.
Email: amzhu@dlut.edu.cn

To improve the photocatalytic activity of TiO₂ film, Ti substrates are irradiated by He ions with different incident ion energy, temperature, and fluence. Anatase TiO₂ films are then coated on the plasma-irradiated substrates via chemical vapor deposition followed by calcination. Photocurrent tests and photocatalytic oxidation (PCO) of formaldehyde are used to assess photocatalytic performance. The optimal plasma-irradiated samples showed a four times higher photocurrent and a three fold increase in the rate constant of the PCO reaction compared to the TiO₂ coated, untreated control sample. It is found that the enhanced photocatalytic activity and photocurrent are related to the changes of Ti crystal structure and surface morphology through plasma irradiation.
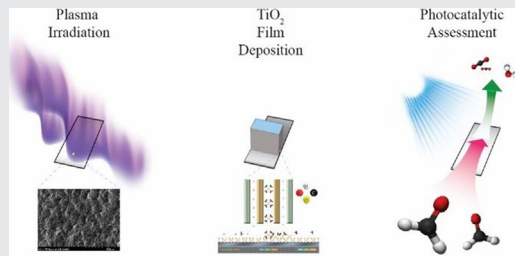
KEYWORDS
ion bombardment, photocatalytic activity, plasma treatment, TiO₂ film, Ti substrate

1 | INTRODUCTION

Energetic He ion (>20 eV) bombardment at 1000–2000 K leads to a formation of fuzz like structures on the surface of tungsten.[1] Other metals such as titanium, copper, and aluminum exhibits similar transformations of their morphologies under He ion bombardment.[2–4] One can tune the generated morphology and their properties by controlling the incident ion energy as well as the temperature of the target metal.[5,6] Plasma irradiation on metal surfaces could cause significant enhancement of the physical properties of the surface,[6,7] and metal substrates like tungsten and titanium were irradiated by plasma for improving photocatalytic performance.[8–11] Kajita et al.[8] reported

enhanced hydrogen production through low-fluence He plasma bombarded Ti substrate with thermally oxidized layer of TiO₂. Moreover, among many photocatalysts, TiO₂ is almost the best one for industrial application of photocatalysis due to its abundance, harmlessness, low cost, and chemical stability. One of the issues that hinders the efficiency of photocatalysis is the recombination of the photo-generated electron-hole pairs (EHP). Much work has been carried out to resolve the issue by doping metals such as Pt, Pd, Cu, Ag, and Au onto TiO₂ in order to bring the metal into contact with TiO₂, where a metal-semiconductor junction forms that promotes charge carrier separation and therefore showed improved performance.[12–18] However, few works studied photocatalytic performance of TiO₂/Ti

system with plasma-irradiated Ti substrate, despite the fact that they form an ohmic junction[19] which facilitates better charge transfer than does a Schottky junction formed by most noble metals with TiO₂.[20] In particular, to the best of our knowledge, the effect of crystal structure change of plasma-irradiated Ti substrate on photocurrent and photocatalytic activity has not yet been reported.

Herein, we report an enhancement of photocatalytic performance of TiO₂/Ti system via high-fluence He plasma irradiation of the Ti substrate prior to TiO₂ coating. The assessment was carried through the photocatalytic oxidation (PCO) of formaldehyde, an indoor air pollutant which can cause "sick building" syndrome,[21,22] into CO_2 under illumination of UV-light.[23–25] Plasma-irradiated Ti substrates showed a maximum of a three-fold increase in the reaction rate constant (k) of formaldehyde PCO. Combined with a photocurrent test and X-ray Diffraction (XRD) and SEM characterizations, we found that the enhanced performance is correlated with the change in crystal structure and surface morphology of Ti substrates caused by plasma irradiation.

2 | EXPERIMENTAL

2.1 | Helium ion irradiation on Ti substrates

The experiment setup for the He ion irradiation of the Ti substrate is shown in Figure 1.[2] A Ti substrate sample (Alfa Aesar, 99% purity) with 1.3 cm (width) × 4.4 cm (length) × 0.05 cm (thickness) was supported by two copper tubes. The copper tubes, where the wires were connected to the substrate, were mounted on a ceramic stage. After placing the bell jar onto the O-ring, the bottom of the ceramic stand was aligned with the bottom of the bell jar. A photo of the setup was shown in Figure 1b.

All four edges of each sample were thoroughly polished to minimize possible arcing at the edge of samples. Samples were exposed to a helicon source helium plasma (MORI 200[26]). Plasma conditions for He ion exposure were similar to those of previous investigation for growth of tungsten and palladium nanostructures[2] with slight variations: input RF power of 700 W, a magnetic field strength of 57 Gauss, a base pressure of 4 mTorr, and helium pressure of 100 mTorr measured by a convectron gauge (Graville Phillips 375). An external bias voltage of −50 to −140 V was applied to the sample to control the incident ion energy, as well as a tunable resistively heating AC current supplied by a variac. Plasma potential near the biased sample was determined by placing an adjacent RF-compensated single Langmuir probe to measure the plasma potential and therefore calculate the incident ion energy. Temperature of the substrate was measured through a K-type thermocouple (Omega) sandwiched between the bolt and the sample. Due to signal interference, bulk temperature was determined by recording the temperature decay after turning off the RF power. Irradiation conditions are shown in Table 1 with all relevant parameters specified. The irradiated samples (uncoated) were observed with a Hitachi S4700 SEM.

2.2 | Deposition and characterization of TiO₂ thin film

After plasma irradiation, samples $(i)_c$–$(vii)_c$ were coated with amorphous TiO₂ film for 15 min via chemical vapor deposition using titanium (IV) isopropoxide (TTIP) and H_2O as the precursors, using a method described previously,[27] then calcined in air atmosphere at 500 °C for 2 h to convert amorphous TiO₂ into the anatase phase.

The plane and cross-section views of the TiO₂ film on the coated samples were investigated with a field-emission SEM
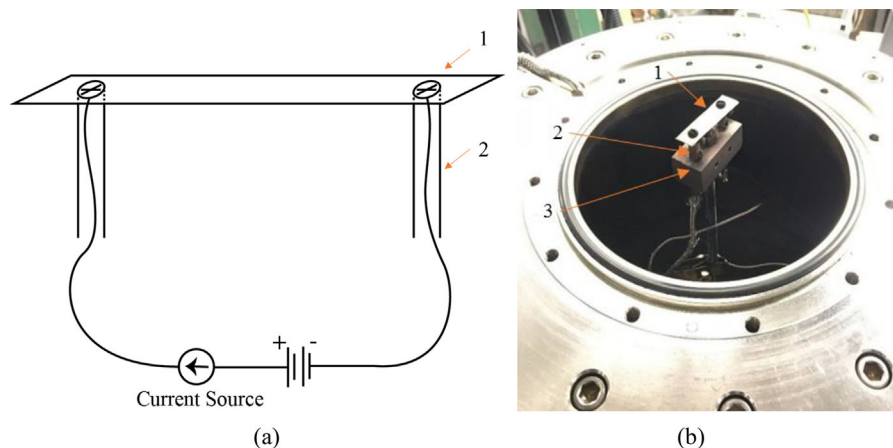

FIGURE 1 a) Schematic diagram and (b) photo of experiment setup. 1. Ti substrate for He ion bombardment; 2. Copper tube to support Ti substrate; 3. Ceramic stage

TABLE 1 Irradiation conditions used in experiments; error estimations of incident ion energy, temperature, and fluence are 2 eV, 5 K, and 16% of reported fluence value, respectively.

Sample label[a]	Incident ion energy/eV	Temperature/ K	Fluence/ ions·cm^{-2}
(i) or (i)$_c$	79	788	2.5×10^{22}
(ii) or (ii)$_c$	109	836	3.9×10^{22}
(iii) or (iii)$_c$	109	885	3.5×10^{22}
(iv) or (iv)$_c$	129	867	3.4×10^{22}
(v) or (v)$_c$	169	876	1.7×10^{22}
(vi) or (vi)$_c$	169	876	3.7×10^{22}
(Untreated)$_c$[b]	–	–	–

The temperature is controlled by the incident ion energy. Fluence is controlled by the time duration of the exposure.

[a]The labels with and without a subscript "c" represent coated and uncoated (the corresponding plasma-treated substrate) samples, respectively.

[b]The coated sample on a substrate without plasma irradiation.

(Nova NanoSEM 450, FEI). X-Ray Diffraction (XRD) was performed on the coated samples via Empyrean (PANalytical); a Co source with wavelength of 1.79 Å was used for XRD.

2.3 | Photocurrent measurement

A photo-electrolysis apparatus was set up for photocurrent testing. Each sample with an active area of $1.3 \times 1.7 \, cm^2$ was clamped with small Pt sheet as a working electrode, immersed in 0.1 M H_2SO_4 solution with a magnetic stir bar. Another Pt sheet serves as a counter electrode; Ag/AgCl with saturated KCl solution served as a reference electrode. The working electrode and the reference electrode were placed in a glass jar with a quartz window of 2.3 cm diameter for UV illumination; the counter electrode was placed in another jar with a proton exchange membrane connecting the two jars. Current was monitored using a GAMRY Reference 600, in which 1 V versus Ag/AgCl was applied. A Xe lamp (emission spectra shown in the previous paper[28]) with a power of 300 W served as a UV light source. From 20–40 s to 60–80 s, UV light was illuminated.

2.4 | Photocatalytic oxidation of formaldehyde

The experimental setup and evaluation technique for PCO of HCHO was described previously.[29] The PCO evaluation at $25 \pm 1 \, °C$ using a UV lamp of 254 nm (TUV 8W, PHILIPS) was conducted according to the following procedure: (a) Initial concentration of HCHO (C_0) determination; (b) Sample purification; (c) PCO reaction; and (d) Initial concentration double checked for accuracy. In step (a), the reactant gas, composed of 51 ± 1 ppm HCHO, 0.50 vol% H_2O and 20% O_2 with the balance N_2, flows into a home-made VOC-to-CO_2

converter, whose CO_x concentration was measured by an IR CO_x analyzer (S710, Sick-Maihak, Germany) to determine C_0. With step (b), O_2 containing 0.50 vol% H_2O was introduced into the PCO reactor under 254 nm illumination for the CO_x concentration to approach a baseline level. In step (c), the reactant gas containing HCHO was introduced into PCO reactor and the CO_x concentration was measured as a function of time-on-stream (TOS). In the last step, C_0 was checked again to ensure accuracy.

With the above setup and conditions, the definitions of residence time (τ) and HCHO conversion (X) are shown in the following equations:

$$\tau = \frac{V}{F} = \frac{Sd}{F} \tag{1}$$

$$X = \frac{C_{CO_2}}{C_0} \times 100\% \tag{2}$$

where V is the effective volume of the PCO reactor, F being the total flow rate (200 mL min^{-1}), S being the area of titania film ($1.3 \times 2.5 \, cm^2$), d (1 mm) being the gap between the sample and quartz window, and C_{CO_2} being the concentration of CO_2 after HCHO PCO.

3 | RESULTS AND DISCUSSION

The most representative morphology is presented in Figure 2 for all samples exposed to the He plasma. As the incidence energy increases from 79 to 169 eV, the morphology transits from spherical particles to valleys of "webs" and eventually to huge hills; morphologies appeared to be bubble-driven like palladium[6] and tungsten[30] from previous work. Comparing (v) and (vi), as the fluence doubles, sputtering effects started dominating, eliminating the porous structures. For sample (ii) and (iii), as temperature increases, the surface started to anneal and holes observable in sample (ii) disappeared; the surface also became roughened, possibly due to more mobile metal atoms caused by the bombardment of He ion of the same incident energy.

The morphology of the coated samples depends upon that of the substrate. Compared with the sample (untreated)$_c$ (Figure 3b), the coated sample (vi)$_c$ exhibits a hill-like morphology (Figure 3a), which is remarkably similar to the uncoated sample (vi) (Figure 2). In Figure 3b, in terms of the morphology of the sample (untreated)$_c$, the top view shows a lot of stress with cracking lines, which may arise from the mechanic processing of the untreated surface of Ti substrate. The TiO_2 film thickness of the coated samples is approximately 150 nm, as shown in Figures 3c and 3d.

Figure 4 shows XRD patterns of the untreated substrate and the coated samples on the untreated and plasma treated
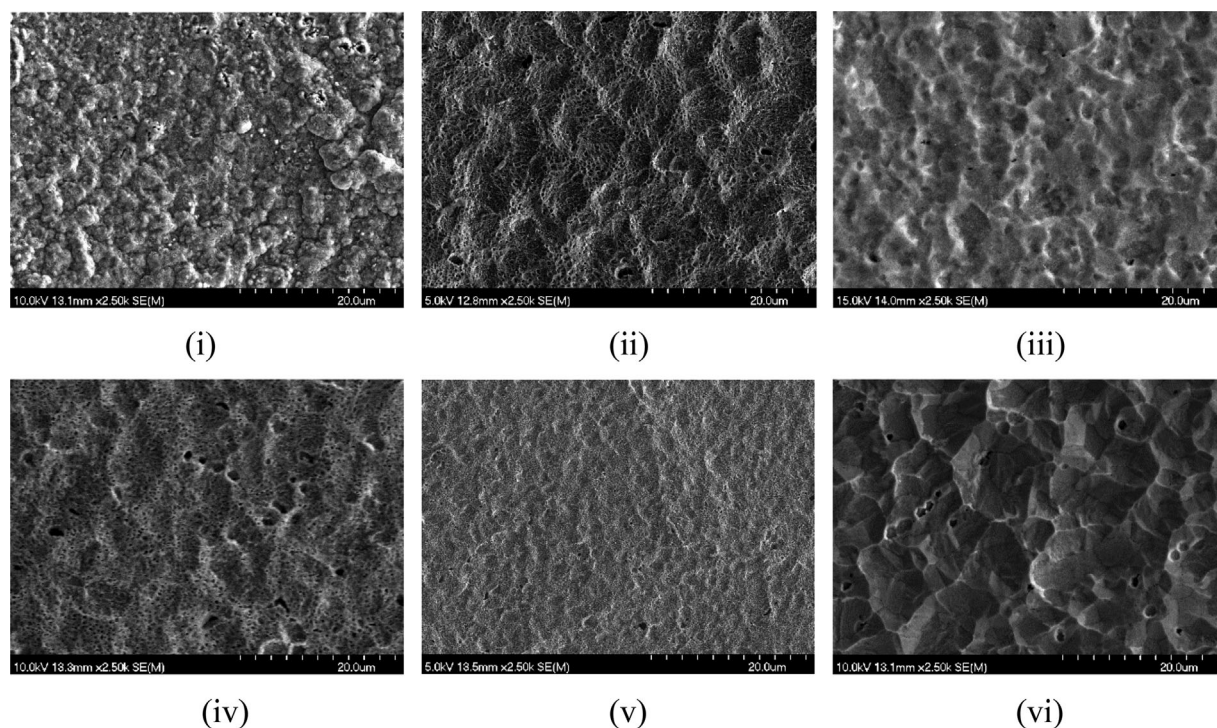
FIGURE 2 Plane-view SEM image of titanium substrate irradiated by He ion prior to TiO$_2$ coating. A morphology evolution was observed: from spherical particles (i) to porous "web," shown in (ii)–(v), and eventually to annealed hills and valleys due to sputtering. From visual inspection, the morphology seemed to be bubble driven. The difference between each sample is shown in Table 1gr2

substrates. The XRD peaks were attributed with reference to JCPDS-ICDD card No. 44-1294 for titanium and JCPDS-ICDD card No. 21-1272 for anatase TiO$_2$. The untreated substrate show typical XRD distribution of Ti. The coated, plasma-untreated sample ((untreated)$_c$) showed a group of

peaks from Ti as well as a peak from anatase TiO$_2$, being the most photochemical active crystalline phase of TiO$_2$. The signal of anatase TiO$_2$ is relatively weak compared with that of Ti, due to its existence as a thin film. The characterization of X-ray photoelectron spectroscopy (XPS) and UV-vis
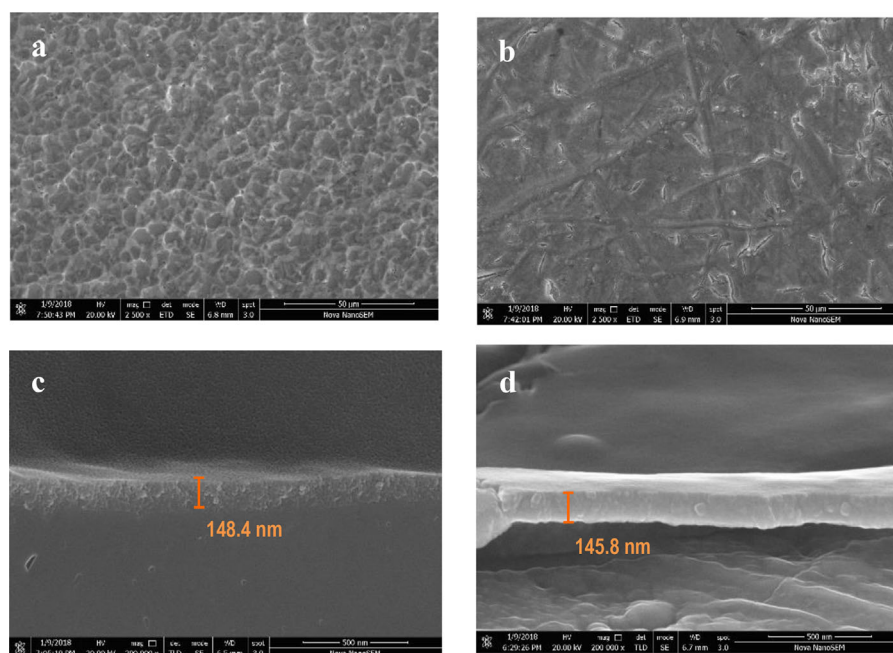

FIGURE 3 Plane-view (a, b) and cross-section (c, d) SEM image of the coated samples (vi)$_c$ (a, c) and (untreated)$_c$ (b, d)
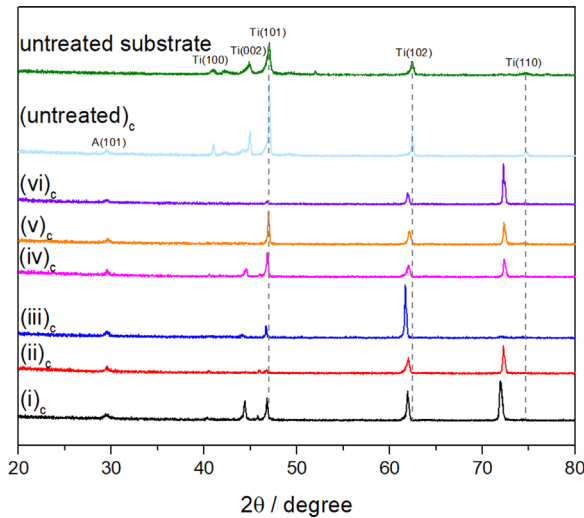
FIGURE 4 XRD spectra of coated samples on untreated and plasma treated substrates. A titanium substrate without plasma treatment (untreated substrate) is used for reference. Ti denotes titanium metal crystalline whereas A denotes anatase TiO₂. Co source with a wavelength of 1.79 Å was used

spectra for the anatase TiO$_2$ films could be found in our previous paper.[31]

A closer look at Figure 4 reveals that not only Ti(110) peaks were shifted, but also Ti(101) and Ti(102) peaks were shifted to have a lower Bragg angle due to the expansion of crystal. The (110) face of Ti, in particular, had shifted to a much lower Bragg angle; the peaks appear to be broadened as well. The former could be explained by the base expansion of hexagonal-closed packed crystal structure by the intrusion of He atoms. The broadening of peaks can also be accounted by inhomogeneous stress produced by infusion of He in Ti. It is worth noting that for some samples, part of characteristic peaks of Ti disappeared completely, such as (110) peak of Ti for sample (iii)$_c$; the disappearance of Ti(110) peak corresponded to the intensification of Ti(102) peak.

To express the variation in the preferred orientation of Ti crystal planes due to plasma irradiation, the texture coefficient (TC) of the plane specified by Miller indices (hkl) can be calculated by the equation below:[32]

$$TC_{(hkl)} = \frac{N \cdot I_{(hkl)}}{I^0_{(hkl)} \cdot \sum \frac{I_{(hkl)}}{I^0_{(hkl)}}} \quad (3)$$

where $I^0_{(hkl)}$ and $I_{(hkl)}$ are the intensities of the (hkl) plane of an untreated Ti substrate and of the coated sample, respectively; N is the total number of reflection planes considered. In Table 2, five planes of Ti(101), Ti(102), Ti(110), Ti(002), and Ti(100) were taken into account and $N = 5$ accordingly. Table 2 lists the value of TC for the five Ti crystal planes of the coated sample. Plasma irradiation causes that the value of $TC_{(101)}$ is much less than 1 and the TC value of other planes is much more than 1 instead. For instance, $TC_{(102)}$ of sample (iii)$_c$ equals 3.4 and $TC_{(110)}$ of sample (vi)$_c$ equals 4.5, which indicates a highly preferred orientation of (102) plane for sample (iii)$_c$ and of (110) plane for sample (vi)$_c$.

Photocurrents generated by UV light illumination for each sample was plotted against time in Figure 5. At time from 20 to 40 s and from 60 to 80 s, samples were illuminated under UV light. The magnitude of photocurrent was repeatable in several cycles with/without UV illumination for all samples. Samples (iv)$_c$ and (v)$_c$ exhibits the highest photocurrent, almost five times that of samples (untreated)$_c$ and (i)$_c$.

Conversion of formaldehyde and the corresponding reaction rate constant for each sample were plotted in Figure 6. The reaction rate constant k can be calculated via Equation 4, where a first order kinetics for oxidation of formaldehyde is obeyed.[29,33] In this experiment, resident time τ equals 0.1 s.
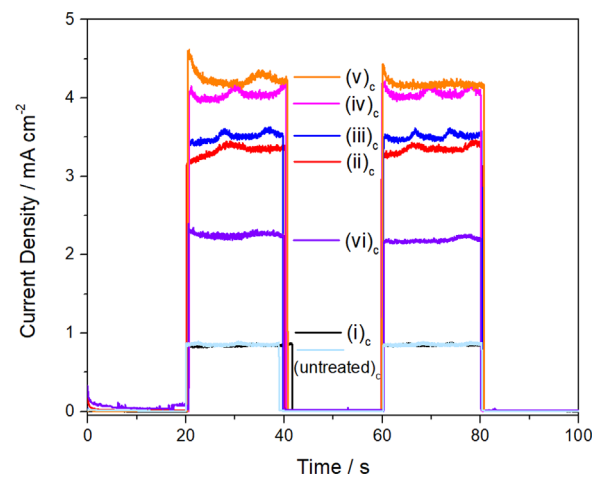

FIGURE 5 Photocurrent of the samples under Xe light illumination under 1 V versus Ag/AgCl. From 20–40 s to 60–80 s, UV light was illuminated. Sample (v)$_c$ and (iv)$_c$ showed four fold higher photocurrent than sample (i)$_c$ and (untreated)$_c$

TABLE 2 Texture coefficient of various Ti crystal plane of each coated sample; estimation of error is within 5% of determined fraction

Sample#	(i)$_c$	(ii)$_c$	(iii)$_c$	(iv)$_c$	(v)$_c$	(vi)$_c$	(Untreated)$_c$
Ti(101)	0.2	0.1	0.4	0.4	0.5	0.1	1.1
Ti(102)	0.6	0.5	3.4	0.5	0.5	0.3	0.8
Ti(110)	3.6	4.1	0.7	3.4	3.7	4.5	1.2

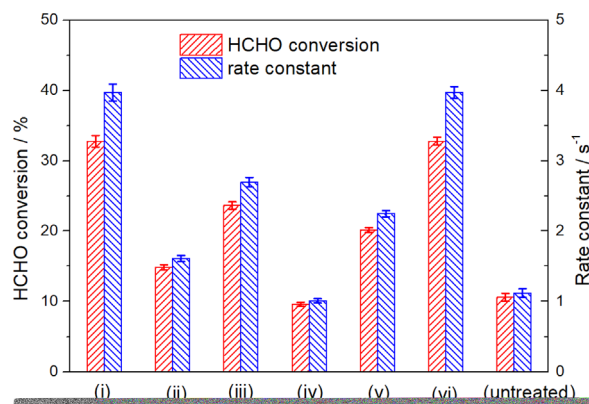**FIGURE 6** HCHO conversion and rate constant of each sample, where the highest rate constant (sample (i)$_c$ and (vi)$_c$) is four times of the TiO$_2$ coated, untreated sample. The PCO evaluation was conducted at 25 ± 1 °C with reactant gas composed of 51 ± 1 ppm HCHO, 0.50 vol% H$_2$O and 20% O$_2$ with the balance of the gas N$_2$. The resident time τ equals 0.1 s

$$\ln(1 - X) = -k\tau \qquad (4)$$

Demonstrated in Figure 6, except for sample (iv)$_c$, all other plasma-irradiated sampled showed higher activity in formaldehyde PCO reaction than the untreated sample. In particular, sample (i)$_c$ and (vi)$_c$ have the highest reaction rate constant, which is four-times of the untreated sample.

These improvements in photocurrent and rate constant are mainly caused by the changes in crystal structure such as texture coefficient and lattice expansion, as well as surface morphology of the He-plasma-irradiated Ti substrate. For photocurrent, if the morphology is grouped into porous samples of (ii)$_c$, (iv)$_c$, and (v)$_c$, hill-valley samples of (iii)$_c$ and (vi)$_c$, and spherical sample of (i)$_c$, we can observe by comparing Tables 2 and 3, that within each group, the higher texture coefficient of the Ti(101) plane a sample has, the higher the photocurrent. Since the magnitude of photocurrent manifests the density of charge carrier in the TiO$_2$/Ti system upon illumination of UV-light, we speculate that the change in crystal texture coefficient of Ti caused by plasma irradiation results in significant changes in the work function[34–36] of Ti substrate, which gives rise to different photocurrents. From the morphology perspective, porous web morphology outperforms the hill-valley morphology and spherical morphology for photocurrent. Although the untreated sample has high Ti(101) composition, we suspect that its low photocurrent may be addressed by its smaller

lattice constant compared to the irradiated ones as well as its relative smooth morphology.

Through examining Table 3, a discrepancy is observed between photocurrent and reaction rate constant, such that the highest photocurrent does not correspond to the highest reaction rate constant and vice versa. As photocurrent can only indicate the density of charge carrier, the rate constant is an overall result of surface species absorption/desorption, surface reaction obeying the Langmuir-Hinshelwood mechanism,[28,29,37] and surface concentration of charge carriers.[38–40] Although we are seeing some relation between crystal texture coefficient and reaction rate constant, as the reaction involves multiple complex processes it is hard to judge. Nevertheless, the effect of morphology is significant, as the presence of highly rough surface made sample (v)$_c$ higher activity than sample (iv)$_c$ despite their similar crystal texture coefficient.

4 | CONCLUSION

Ti substrates were treated with high-fluence He plasma under different incident energy, temperature, and fluence conditions. TiO$_2$ thin films were deposited on each substrate, followed by calcination to form an anatase phase. Samples were characterized by SEM, XRD, photocurrent test, and evaluated through PCO of formaldehyde. Overall, the chemical performance of plasma-treated sample was three to four times better than a TiO$_2$ thin-film-deposited, nonirradiated Ti sample. It was suggested that the enhanced photocatalytic activity and photocurrent are related to the changes of crystal structure and surface morphology of Ti substrate through plasma irradiation. This work not only indicates that plasma irradiated material could offer a huge improvement in the field of photocatalysis, but also that the performance of TiO$_2$ film can be modulated through tuning plasma processing parameters.

ORCID

Wei-Kun Zhu (iD) http://orcid.org/0000-0002-0828-3645
Ai-Min Zhu (iD) http://orcid.org/0000-0002-4527-6372

REFERENCES

[1] S. Takamura, N. Ohno, D. Nishijima, S. Kajita, *Plasma Fusion Res.* **2006**, *1*, 051.
[2] P. Fiflis, N. Connolly, D. N. Ruzic, *J. Nucl. Mater.* **2016**, *482*, 201.

TABLE 3 Comparison of the samples in photocurrent and rate constant

Sample#	(i)$_c$	(ii)$_c$	(iii)$_c$	(iv)$_c$	(v)$_c$	(vi)$_c$	(Untreated)$_c$
Photocurrent/mA · cm^{-2}	0.85	3.4	3.5	4.1	4.2	2.2	0.85
Rate constant/s^{-1}	4.0	1.6	2.7	1.0	2.2	4.0	1.1

[3] I. Tanyeli, L. Marot, D. Mathys, M. C. van de Sanden, G. De Temmerman, *Sci. Rep*. **2015**, *5*, 9779.

[4] S. Kajita, D. Kitaoka, N. Ohno, R. Yoshihara, N. Yoshida, T. Yoshida, *Appl. Surf. Sci*. **2014**, *303*, 438.

[5] M. J. Baldwin, R. P. Doerner, *Nucl. Fusion* **2008**, *48*, 035001.

[6] P. Fiflis, M. P. Christenson, N. Connolly, D. N. Ruzic, *Nanomaterials* **2015**, *5*.

[7] M. Yajima, Y. Hatano, S. Kajita, J. Shi, M. Hara, N. Ohno, *J. Nucl. Mat*. **2013**, *438*, S1142.

[8] S. Kajita, T. Yoshida, N. Ohno, T. Ishida, D. Kitaoka, *Jpn. J. Appl. Phys*. **2016**, *55*, 106202.

[9] K. Komori, T. Yoshida, T. Nomoto, M. Yamamoto, C. Tsukada, S. Yagi, M. Yajima, S. Kajita, N. Ohno, *Nucl. Instrum. Methods Phys. Res. B* **2015**, *365*, 35.

[10] K. Komori, T. Yoshida, S. Yagi, H. Yoshida, M. Yajima, S. Kajita, N. Ohno, *e-J. Surf. Sci. Nanotechnol*. **2014**, *12*, 343.

[11] S. Kajita, T. Yoshida, D. Kitaoka, R. Etoh, M. Yajima, N. Ohno, H. Yoshida, N. Yoshida, Y. Terao, *J. Appl. Phys*. **2013**, *113*, 134301.

[12] T. Hirakawa, P. V. Kamat, *J. Am. Chem. Soc*. **2005**, *127*, 3918.

[13] Y. Tian, T. Tatsuma, *J. Am. Chem. Soc*. **2005**, *127*, 7632.

[14] E. Kowalska, H. Remita, C. Colbeau-Justin, J. Hupka, J. Belloni, *J. Phys. Chem. C* **2008**, *112*, 1124.

[15] O. Tahiri Alaoui, A. Herissan, C. Le Quoc, M. e. M. Zekri, S. Sorgues, H. Remita, C. Colbeau-Justin, *J. Photochem. Photobiol*. **2012**, *242*, 34.

[16] E. Grabowska, A. Zaleska, S. Sorgues, M. Kunst, A. Etcheberry, C. Colbeau-Justin, H. Remita, *J. Phys. Chem. C* **2013**, *117*.

[17] Z. Hai, N. El Kolli, B. D. Uribe, P. Beaunier, M. Jose-Yacaman, J. Vigneron, A. Etcheberry, S. Sorgues, C. Colbeau-Justin, J. Chen, H. Remita, *J. Mater. Chem. A* **2013**, *1*, 10829.

[18] P. Christopher, H. Xin, S. Linic, *Nat. Chem*. **2011**, *3*, 467.

[19] F. Hossein-Babaei, S. Rahbarpour, *Solid-State Electron*. **2011**, *56*, 185.

[20] F. Hossein-Babaei, M. M. Lajvardi, N. Alaei-Sheini, *Appl. Phy. Lett*. **2015**, *106*, 083503

[21] P. Chin, L. Yang, D. Ollis, *J. Catal*. **2006**, *237*, 29.

[22] D. Z. Zhao, X. S. Li, C. Shi, H. Y. Fan, A. M. Zhu, *Chem. Eng. Sci*. **2011**, *66*, 3922.

[23] A. L. Linsebigler, G. Lu, J. T. Yates, *Chem. Rev*. **1995**, *95*, 735.

[24] S. Sun, J. Ding, J. Bao, C. Gao, Z. Qi, C. Li, *Catal. Lett*. **2010**, *137*, 239.

[25] J. Yang, D. Li, Z. Zhang, Q. Li, H. Wang., *J. Photochem. Photobiol. A: Chem*. **2000**, *137*, 197.

[26] R. Tobe, A. Sekiguchi, M. Sasaki, O. Okada, N. Hosokawa, *Thin Solid Films* **1996**, *281-282*, 155.

[27] Z. G. Sun, X. S. Li, X. Zhu, X. Q. Deng, D. L. Chang, A. M. Zhu, *Chem. Vap. Deposition* **2014**, *20*, 8.

[28] X. Q. Deng, J. L. Liu, X. S. Li, B. Zhu, X. Zhu, A. M. Zhu, *Catal. Today* **2017**, *281*, 630.

[29] X. Zhu, D. L. Chang, X. S. Li, Z. G. Sun, X. Q. Deng, A. M. Zhu, *Chem. Eng. J*. **2015**, *279*, 897.

[30] P. Fiflis, D. Curreli, D. N. Ruzic, *Nucl. Fusion* **2015**, *55*, 033020.

[31] X. Q. Deng, X. Zhu, Z. G. Sun, X. S. Li, J. L. Liu, C. Shi, A. M. Zhu, *Chem. Eng. J*. **2016**, *306*, 1001.

[32] T. W. Cornelius, J. Brötz, N. Chtanko, D. Dobrev, G. Miehe, R. Neumann, M. E. T. Molares, *Nanotechnol*. **2005**, *16*, S246.

[33] H. Liu, Z. Lian, X. Ye, W. Shangguan, *Chemosphere* **2005**, *60*, 630.

[34] A. R. Kumarasinghe, W. R. Flavell, A. G. Thomas, A. K. Mallick, D. Tsoutsou, C. Chatwin, S. Rayner, P. Kirkham, S. Warren, S. Patel, P. Christian, P. O'Brien, M. Gratzel, R. Hengerer, *J. Chem. Phys*. **2007**, *127*, 114703.

[35] G. Xiong, R. Shao, T. C. Droubay, A. G. Joly, K. M. Beck, S. A. Chambers, W. P. Hess, *Adv. Funct. Mater*. **2007**, *17*, 2133.

[36] T. Li, B. L. Rickman, W. A. Schroeder, *Phys. Rev. Accel. Beams* **2015**, *18*, 073401.

[37] W. H. Ching, M. Leung, D. Y. C. Leung, *Sol. Energy* **2004**, *77*, 129.

[38] Z. Zhang, J. T. Yate, Jr., *Chem. Rev*. **2012**, *112*, 5520.

[39] Z. Zhang, J. T. Yate, Jr., *J. Phys. Chem. Lett*. **2010**, *1*, 2185.

[40] S. Ma, M. E. Reish, Z. Zhang, I. Harrison, J. T. Yate, Jr., *J. Phys. Chem. C* **2017**, *121*, 1263.